J. Plasma Physics (2003), *vol.* 69, *part* 5, *pp.* 383–395. © 2003 Cambridge University Press
DOI: 10.1017/S002237780300223X Printed in the United Kingdom

Microinstabilities excited by energetic ring current protons

S. MOOLLA[1] and R. BHARUTHRAM[2]

[1]Department of Physics, University of Durban-Westville, Durban, South Africa
[2]Director of Research, University of Natal, Durban 4001, South Africa
(Bharuthramr@nu.ac.za)

(Received ???)

Abstract. It is well known that energetic protons having a ring-type, anisotropic velocity distribution can generate low-frequency electromagnetic waves, propagating nearly transverse to the geomagnetic field lines, in the ring current region of the Earth's magnetosphere by exciting mode 1 and mode 2 non-resonant instabilities and a resonant instability. In this paper, detailed investigations of the resonant and non-resonant instabilities are conducted as a function of plasma parameters such as ring speeds, electron temperatures, magnetic field strength and wave propagation directions. Our analysis is for parameters corresponding to the ring current region of the Earth's magnetosphere.

1. Introduction

The outer layer of the Sun (called the solar corona) is not in static equilibrium. As a result, it wavers and expands into outer space and interacts with both magnetized and unmagnetized bodies. The Earth, being magnetized ensures that this interaction induces large-scale currents which can almost confine the planetary magnetic field. Thus, a major magnetic structure called a magnetosphere is formed around the Earth (Parks 1991).

Particle data from Explorer 45, AMPTE/CCE, GEOS 1 and 2 and other spacecraft clearly indicate the presence of energetic (hot) proton distributions in the ring current region of the Earth's magnetosphere (Fritz and Spjeldvik 1979; Perraut et al. 1982; Kistler et al. 1990; Laakso et al. 1990; Lui et al. 1990). The trapped particles in the Earth's magnetosphere move under the action of the Lorentz force. In addition to the usual cyclotron motion, the particles travel in the North–South direction.

The inhomogeneous planetary magnetic field also forces the trapped particles to drift in the azimuthal direction with a drift $\mathbf{v}_{\nabla B} = \frac{1}{2}\frac{mv_\perp^2}{qB}\frac{\mathbf{B}\times\nabla\mathbf{B}}{B^2}$, where m is the particle mass, q is the charge of the particle ($q = +e, -e$ for a proton, electron) and $v_\perp$ is the particle velocity perpendicular to the magnetic field $\mathbf{B}$. This drift is charge-dependent and electrons and ions drifting in the opposite direction create a large-scale current, called a ring current, which lies within the plasma sheet region of the Earth's magnetosphere.

The relative drift between electrons and ions due to the ring current provides a source of free energy to excite linear plasma instabilities. In addition, the velocity

https://doi.org/10.1017/S002237780300223X Published online by Cambridge University Press

distributions of the charged particles in the ring current region are found to be anisotropic (Singh et al. 1996), which also serves as a source for microinstabilities.

In this paper we examine microinstabilities excited by ring current protons having a given anisotropic ring-type velocity distribution, by extending the parameter study of Singh et al. (1996). Both resonant and non-resonant instabilities are considered.

2. The dispersion relation

We model the ring current region following Singh et al. (1996) by a plasma system consisting of electrons, cold protons and energetic protons (hot) embedded in the geomagnetic field which we treat as uniform, i.e. $\mathbf{B}_0 = B_0\hat{z}$.

Let the equilibrium number density and temperature of the electrons be N_{0e} and T_e, and of the cold protons N_{0c} and T_c, respectively. For quasi-neutrality, $N_{0e} = N_{0c} + N_{0h}$, where N_{0h} is the equilibrium density of the hot protons. The electrons and cold protons have Maxwellian velocity distributions,

$$f_{0e,c} = \frac{N_{0e,c}}{\pi^{3/2} v_{te,c}^{3/2}} \exp\left(-\frac{v^2}{v_{te,c}^2}\right), \tag{1}$$

where $v_{te,c} = (2T_{e,c}/m_{e,i})^{1/2}$ are the thermal velocities of the electrons and cold protons, respectively. We consider the hot protons to have a ring-like distribution function (McClements and Dendy 1994),

$$f_{0h} = \frac{N_{0h}}{2\pi^2 u \alpha_{\parallel h} \alpha_{\perp h} R} \exp\left[-\frac{v_\parallel^2}{\alpha_{\parallel h}^2} - \frac{(v_\perp - u)^2}{\alpha_{\perp h}^2}\right], \tag{2}$$

where u is the mean perpendicular velocity of the ring, $\alpha_\perp$ ($\alpha_{\parallel h}$) are the perpendicular (parallel) thermal velocity of the hot protons and R is a normalization factor given by

$$R = \frac{1}{2\pi^{1/2}} \left\{ \sqrt{\pi} \left[1 + \mathrm{erf}\left(\frac{u}{\alpha_{\perp h}}\right)\right] + \frac{\alpha_{\perp h}}{u} \exp\left(-\frac{u^2}{\alpha_{\perp h}^2}\right) \right\}. \tag{3}$$

Here $\mathrm{erf}(u/\alpha_{\perp h})$ is the error function with argument $u/\alpha_{\perp h}$. A dispersion relation for the ring current instability is obtained by making the following assumptions (Singh et al. 1996). We consider waves that propagate nearly transverse to the ambient magnetic field, i.e. $k_\parallel^2 \ll k_\perp^2$, where $\mathbf{k}_\parallel$ ($\mathbf{k}_\perp$) is the component of the wavevector $\mathbf{k}$ parallel (perpendicular) to $\mathbf{B}_0$. The background electrons and protons are taken as cold, i.e. $\omega/k_\parallel v_{te,c} \gg 1$. We consider frequencies in the range $\omega_{ci}^2 \ll \omega^2 \ll \omega_{ce}^2$, where ω_{ci} (ω_{ce}) is the ion (electron) cyclotron frequency. Under these conditions, the electrons are strongly affected by the magnetic field while the protons are largely unaffected by it. Then for wave perturbations varying as $\exp[-i(\omega t - \mathbf{k}\cdot\mathbf{r})]$, where $\omega = \omega_r + i\gamma$ is the wave frequency, the dispersion relation for the ring current instability, as obtained by solving the linearized Vlasov equation along with the full set of Maxwell's equations, turns out to be (Bhatia and Lakhina 1980; Singh et al. 1996)

$$D(\omega, k) = P - Q\frac{k_\parallel^2}{k^2}\frac{\omega_{pe}^2}{\omega^2} - \frac{\omega_{pc}^2}{\omega^2} + \chi_h = 0, \tag{4}$$

https://doi.org/10.1017/S002237780300223X Published online by Cambridge University Press

where

$$P = 1 + \frac{\omega_{pe}^2}{\omega_{ce}^2}\left[\frac{1 - I_0\exp(-\lambda_e)}{\lambda_e}\right] + \frac{\omega_{pe}^2}{\omega_{ce}^2}\frac{\omega_{pe}^2}{c^2k^2}\left[\frac{\{[I_0(\lambda_e) - I_1(\lambda_e)]\exp(-\lambda_e)\}^2}{1 + \beta_e\exp(-\lambda_e)[I_0(\lambda_e) - I_1(\lambda_e)]}\right] \tag{5}$$

$$Q = \frac{I_0(\lambda_e)\exp(-\lambda_e)}{\left[1 + \frac{\omega_{pe}^2}{c^2k^2}I_0(\lambda_e)\exp(-\lambda_e)\right]} \tag{6}$$

and χ_h is the susceptibility of the hot proton given by

$$\chi_h = \frac{\omega_{ph}^2}{k^2N_{0h}}\int_0^{2\pi}\int_{-\infty}^{\infty}\int_0^{\infty}\frac{\mathbf{k}\cdot\frac{\partial f_{0h}}{\partial \mathbf{v}}}{\omega - \mathbf{k}\cdot\mathbf{v}}\,d\theta\,dv_\parallel\,v_\perp\,dv_\perp. \tag{7}$$

In (4)–(7), $\omega_{pj} = (4\pi N_{0j}e^2/m_j)^{1/2}$ is the plasma frequency and $\omega_{cj} = (eB/m_jc)$ is the cyclotron frequency of the jth species, where $j = e, c$ and h for the electrons, cold protons and hot protons, respectively, $\beta_e = (8\pi N_{0e}kT_e/B_0^2)$ is the plasma beta for electrons, and $I_0(\lambda_e)$ and $I_1(\lambda_e)$ are the modified Bessel functions with argument $\lambda_e = k_\perp^2v_{te}^2/2\omega_{ce}^2$ and c is the speed of light. The term ω_{pe}^2/c^2k^2 appearing in (4) and (5) describes the electromagnetic effects on the electrons. In the limit $\omega_{pe}^2/c^2k^2 \to 0$, the electromagnetic effects disappear and the electron response to the perturbation field becomes strictly electrostatic. We shall now discuss the dispersion relation (4) for some cases where χ_h reduces to some simple forms.

3. The non-resonant instability

On substituting for f_{0h} from (2) in (7) for χ_h, making use of the assumption $k_\parallel \ll k_\perp$ and doing the integration, we obtain

$$\chi_h = -\frac{\omega_{ph}^2}{\sqrt{\pi}uk_\perp\alpha_{\perp h}R}\frac{\partial}{\partial\omega}\left[\int_{-u/\alpha_{\perp h}}^{\infty}\frac{(u + \alpha_{\perp h}x)}{x - \zeta}\exp(-x^2)\,dx\right], \tag{8}$$

where $x = (v_\perp - u)/\alpha_{\perp h}$ and $\zeta = (\omega - k_\perp u)/k_\perp\alpha_{\perp h}$. In the (non-resonant) limit $\zeta \gg x$, one may neglect the pole contributions. Then the expression for the hot proton susceptibility attains a simple form, namely, $\chi_h = -\omega_{ph}^2/(\omega - k_\perp u)^2$. Substituting this value of χ_h into (4) reduces the dispersion relation to (Singh et al. 1996)

$$(\omega^2 - \omega_a^2)\left[(\omega - k_\perp u)^2 - \omega_b^2\right] = \omega_a^2\omega_b^2 \tag{9}$$

where $\omega_a = \frac{\omega_{pc}}{\sqrt{P}}\left[1 + Q\frac{k_\parallel^2\omega_{pe}^2}{k^2\omega_{pc}^2}\right]^{1/2}$ and $\omega_b = \omega_{ph}/\sqrt{P}$.

3.1. Mode 1: non-resonant instability

For $u \approx \omega_b/k_\perp$, we obtain an unstable root of (9):

$$\omega = \left(\frac{\omega_a^2\omega_b}{2}\right)^{1/3}\frac{(1 + i\sqrt{3})}{2} \tag{10}$$

provided $\omega_a^2/\omega_b^2 < 2$. The excitation of this mode demands $N_{0c}/N_{0h} \ll 1$, therefore this mode could be excited when the ring current is far away from the plasmapause,

https://doi.org/10.1017/S002237780300223X Published online by Cambridge University Press

where the population of the cold protons is much smaller than that of the hot component.

3.2. Mode 2: non-resonant instability

For $\omega \approx k_\perp u + \eta$, where $u = \omega_a/k_\perp$ and $\eta \ll \omega_a$, the solution of (9) gives an unstable root with (Singh et al. 1996)

$$\omega_r = \omega_a + \left(\frac{\omega_b^2 \omega_a}{2}\right)^{1/3} \tag{11}$$

and

$$\gamma = \frac{\sqrt{3}}{2}\left(\frac{\omega_b^2 \omega_a}{2}\right)^{1/3} \tag{12}$$

provided $\omega_b^2/\omega_a^2 < 2$. The excitation of this mode requires $N_{0c}/N_{0h} \gg 1$. This means that the presence of a large number of cold protons would facilitate the generation of this mode.

4. The resonant instability

For the non-resonant instability, we neglected the contribution from the pole at $x = \zeta$ in (8) for χ_h. For the resonant instability this contribution is important. Taking into account the effect of the singularity, the susceptibility for the hot protons, in the limit $x \gg \zeta$ can be written as

$$\chi_h = \Re\chi_h + i\Im\chi_h \tag{13}$$

where

$$\Re\chi_h = \frac{2\omega_{ph}^2}{\pi^{1/2}k^2 u\alpha_{\perp h}R}\left[\frac{1}{2}\exp\left(-\frac{u^2}{\alpha_{\perp h}^2}\right) + \frac{\omega}{k_\perp\alpha_{\perp h}}\left\{\frac{\sqrt{\pi}}{2}\left[1 + \mathrm{erf}\left(\frac{u}{\alpha_{\perp h}}\right)\right]\right.\right.$$
$$\left.\left. + \frac{(\omega - k_\perp u)}{k_\perp\alpha_{\perp h}}\frac{1}{2}E_1\left(\frac{u^2}{\alpha_{\perp h}^2}\right) - 2\pi^{1/2}R\left(\frac{\omega - k_\perp u}{k_\perp\alpha_{\perp h}}\right)^2\right\}\right] \tag{14}$$

and

$$\Im\chi_h = \frac{2\pi^{1/2}\omega(\omega - k_\perp u)\omega_{ph}^2}{k_\perp^2 k^2 u\alpha_{\perp h}^3 R}\exp\left[-\left(\frac{\omega - k_\perp u}{k_\perp\alpha_{\perp h}}\right)^2\right], \tag{15}$$

where E_1 is the exponential integral function (Abramowitz and Stegun 1964). Substituting for χ_h in (4), the dispersion relation becomes

$$D_r(\omega, k) + iD_i(\omega, k) = 0 \tag{16}$$

where

$$D_r(\omega, k) = P - Q\frac{k_\parallel^2\omega_{pe}^2}{k^2\omega^2} - \frac{\omega_{pc}^2}{\omega^2} + \Re\chi_h \tag{17}$$

and

$$D_i(\omega, k) = \Im\chi_h. \tag{18}$$

The contribution from the term $\Re\chi_h$ is usually much smaller than the rest of the terms in (17). Therefore, this term can be ignored while calculating the real frequency from $D_r(\omega, k) = 0$. For the case $\gamma/\omega_r \ll 1$, the real frequency and growth

https://doi.org/10.1017/S002237780300223X Published online by Cambridge University Press

rate are given by (Singh et al. 1996)

$$\omega_r \approx \frac{\omega_{pc}}{\sqrt{P}}\left(1+Q\frac{k_\parallel^2\omega_{pe}^2}{k^2\omega_{pc}^2}\right)^{1/2} \tag{19}$$

$$\gamma \approx -\frac{\sqrt{\pi}\omega_r^2(\omega_r-k_\perp u)\omega_{ph}^2}{k_\perp^2 k^2 u\alpha_{\perp h}^2 RP}\exp\left[-\left(\frac{\omega_r-k_\perp u}{k_\perp\alpha_{\perp h}}\right)^2\right]. \tag{20}$$

Detailed numerical solutions of the dispersion relations derived above are presented in the next section as functions of plasma parameters.

5. Results and discussion

The analysis in the previous section has shown that two types of non-resonant instabilities and a resonant instability can be excited in the ring current region by the energetic protons having ring-like velocity distribution functions. Each instability will now be discussed in detail for certain plasma parameters.

5.1. Mode 1 non-resonant instability (M-1NRI)

Standard parameter values used for this instability are (Singh et al. 1996): $\theta \approx 90°$; $T_e = T_h = 200\,\text{eV}$; $B_0 = 80\,\text{nT}$ ($\omega_{ci} = 7.7$ rad s^{-1}); $N_{0c} = 0.01\,\text{cm}^{-3}$; $N_{0h} = 1.6\,\text{cm}^{-3}$, where $\theta = \theta(\mathbf{k}, \mathbf{B}_0) = \cos^{-1}(k_\parallel/k)$. It is recalled that for this mode, we require $N_{0c} \ll N_{0h}$. The dispersion relation (9), which is cubic in ω is solved numerically to present the results that follow. The instability is observed for almost perpendicular propagation of the wave, i.e. for $\cos\theta = k_\parallel/k \approx 0.002$. We note that for the M-1NRI, the growth rate is larger than the real frequency, as was found by Singh et al. (1996). This is also shown by the approximate analytical result in (10), where $\gamma = \sqrt{3}\omega_r$ attests to the very rapid growth of this instability.

Figures 1 and 2 display the behaviour of ω_r and γ with the electron temperature T_e. Both the real frequency and growth rate decrease (for a particular $\lambda_e = k_\perp^2 v_{te}^2/2\omega_{ce}^2$) as the electron temperature increases. Singh et al. (1996) set $T_e = 200\,\text{eV}$, for which γ is significantly smaller than that for $T_e = 100\,\text{eV}$ for the lower λ_e values. These figures indicate real frequencies of $f_r = 1.6$–3.8 Hz and growth rates of $f_\gamma = 2.6$–6.5 Hz for an electron temperature of 100 eV. The decrease in growth rate with increasing T_e may be associated with the fact that as T_e increases, the 'spread' in the electron velocity distribution hinders the charge bunching mechanism that drives the instability.

Real frequency and growth rate dependence on the magnetic field strength are shown in Figs 3 and 4, respectively. For low values of λ_e (i.e. long wavelengths), both ω_r and γ increase with an increase in $|\mathbf{B}_0|$. This behaviour may be explained as follows. As $|\mathbf{B}_0|$ increases, the magnetized particles are more strongly tied to the field lines. Therefore, their motion in the direction of wave propagation (almost perpendicular to $\mathbf{B}_0$) to neutralize the potential perturbations is restricted, thereby enhancing the instability.

5.2. Mode 2 non-resonant instability (M-2NRI)

The assumptions made during the analysis of mode 2 non-resonant instability, are satisfied by the following standard parameters: $\theta \approx 80°$; $T_e = T_h = 200\,\text{eV}$; $B_0 = 320\,\text{nT}$ ($\omega_{ci} = 30.7$ rad s^{-1}); $N_{0c} = 65\,\text{cm}^{-3}$;$N_{0h} = 1.6\,\text{cm}^{-3}$. This instability is found to be excited for propagation directions relative to $\mathbf{B}_0$ around 10° less than

https://doi.org/10.1017/S002237780300223X Published online by Cambridge University Press

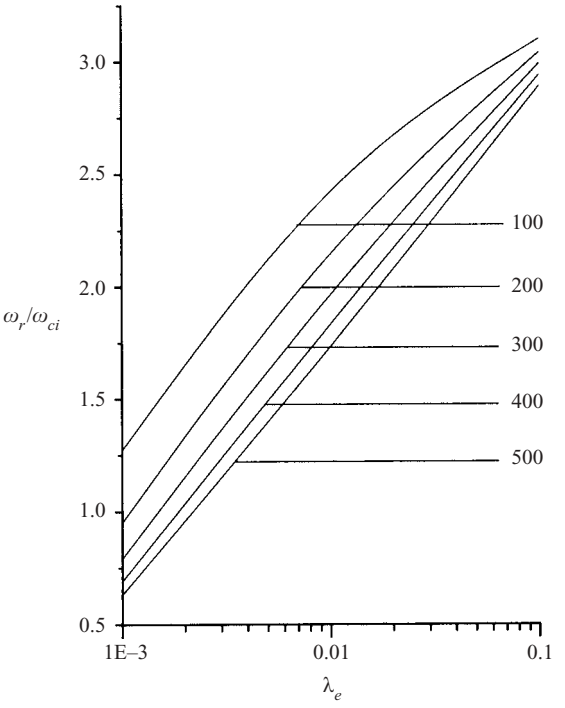


Figure 1. A plot of the normalized real frequency ω_r/ω_{ci} vs $\lambda_e = k_\perp^2 v_{te}^2/2\omega_{ce}^2$, for the M-1NRI. The parameter labelling the curves is the electron temperature T_e in eV.

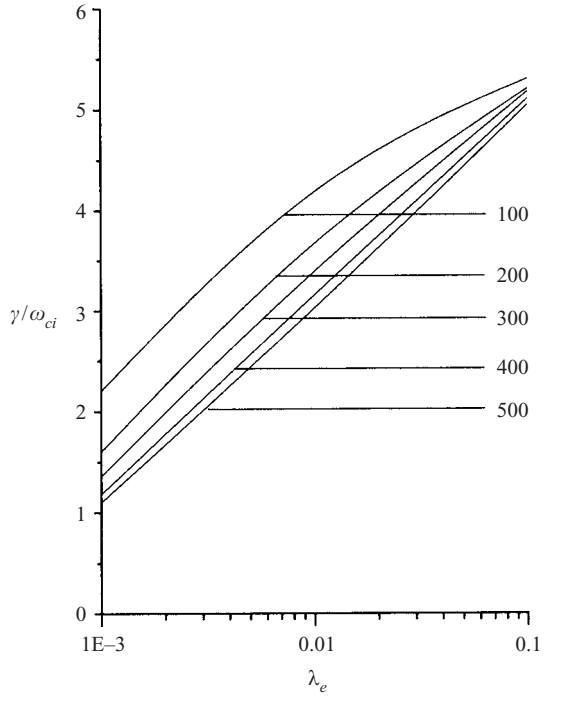


Figure 2. The growth rate curves corresponding to Fig. 1.

https://doi.org/10.1017/S002237780300223X Published online by Cambridge University Press

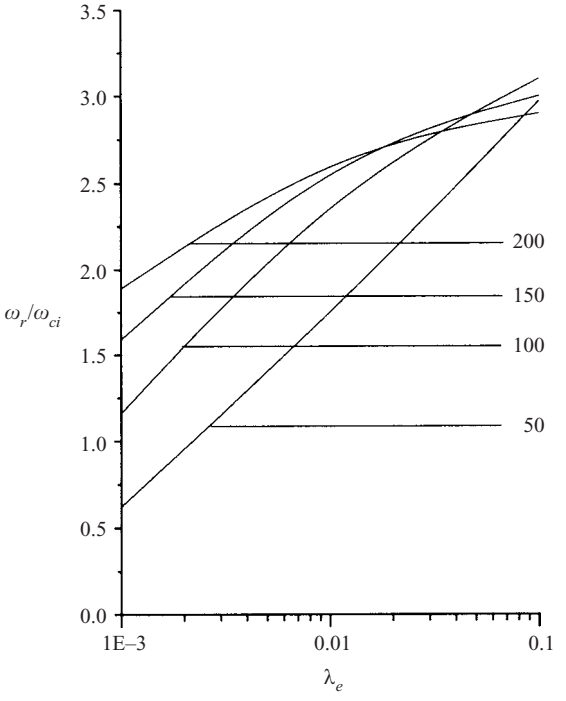


Figure 3. A plot of normalized ω_r vs λ_e for different magnetic field strengths in nT, for the M-1NRI.

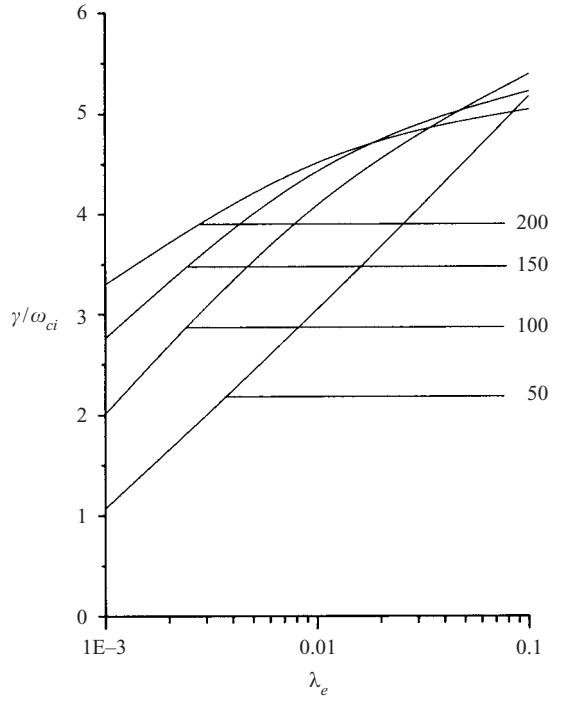


Figure 4. The growth rate curves corresponding to Fig. 3.

https://doi.org/10.1017/S002237780300223X Published online by Cambridge University Press

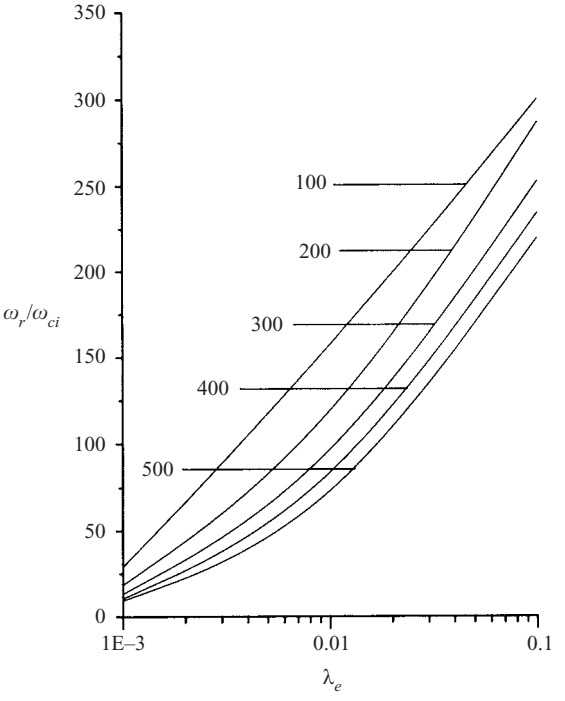


Figure 5. A plot of the normalized real frequency ω_r vs λ_e for the M-2NRI. The parameter labelling the curves is the electron temperature T_e in eV.

those for the above mode which implies that the wavevector has a larger cone of propagation about $\mathbf{k}_\perp$. Previous investigations of this mode by Singh et al. (1996), showed that propagation angles around 80° give results that compare well with observed real frequencies and growth rates.

Figures 5 and 6 show the range of real frequencies and growth rates for various electron temperature values. For $T_e = 300\,\text{eV}$, real frequencies of $f_r = 88$–$1235\,\text{Hz}$ and growth rates of $f_\gamma = 10$–$68\,\text{Hz}$ are obtained. The behaviour with T_e is similar to that for the M-1NRI. However, in contrast to Fig. 1, the spread in ω_r and γ is larger for higher values of λ_e. The variation in the magnitudes of ω_r and γ over the chosen range of λ_e values is very much wider in the case of M-2NRI. In addition, the real frequency and growth rate for the M-2NRI are at least two orders of magnitude larger than those for the M-1NRI for the selected range of values.

The variation of the real frequency with the strength of the magnetic field is similar to that found for the M-1NRI (Fig. 3). However, the variation of the growth rate is more dramatic, as can be seen from Fig. 7, as compared with Fig. 4. Also, we note that for the M-2NRI, $\omega_r > \gamma$, a behaviour opposite to that of the M-1NRI.

Figures 8 and 9 show solutions of the general dispersion relation (9) for the chosen parameters corresponding to the assumptions for mode 1 non-resonant instability (M-1NRI) and mode 2 non-resonant instability (M-2NRI), respectively, as well as intermediate parameters corresponding to an intermediate mode (M-INRI). The real frequencies of the M-INRI lie close to the M-2NRI with a notable cross-over in real frequency as λ_e increases. However, the growth rate of the M-INRI dominates the growth rates of both the M-1NRI and M-2NRI.

https://doi.org/10.1017/S002237780300223X Published online by Cambridge University Press

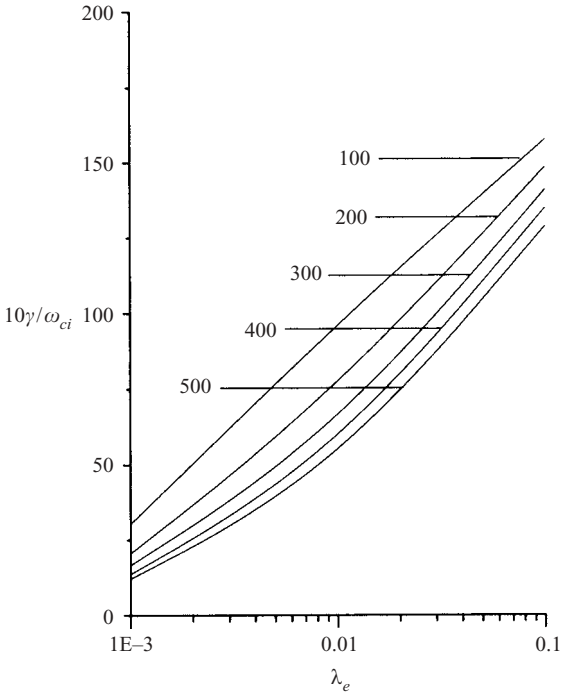


Figure 6. The growth rate curves corresponding to Fig. 5.

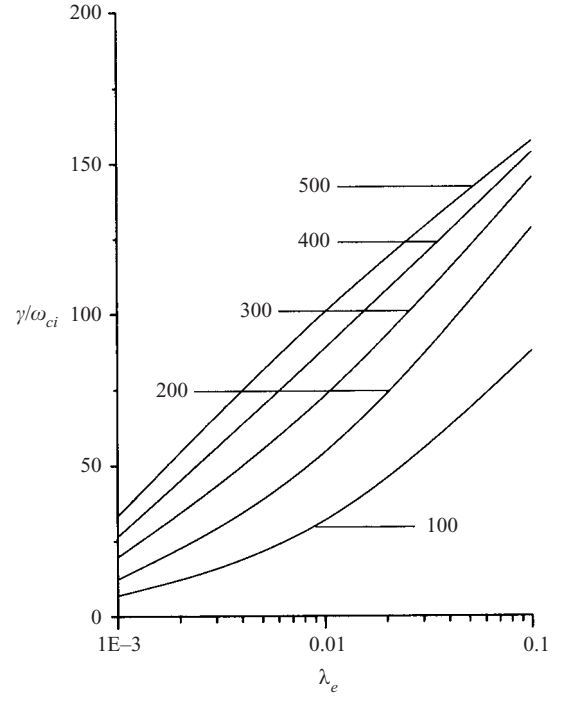


Figure 7. A plot of the normalized γ vs λ_e for different magnetic field strengths in nT, for the M-2NRI.

https://doi.org/10.1017/S002237780300223X Published online by Cambridge University Press

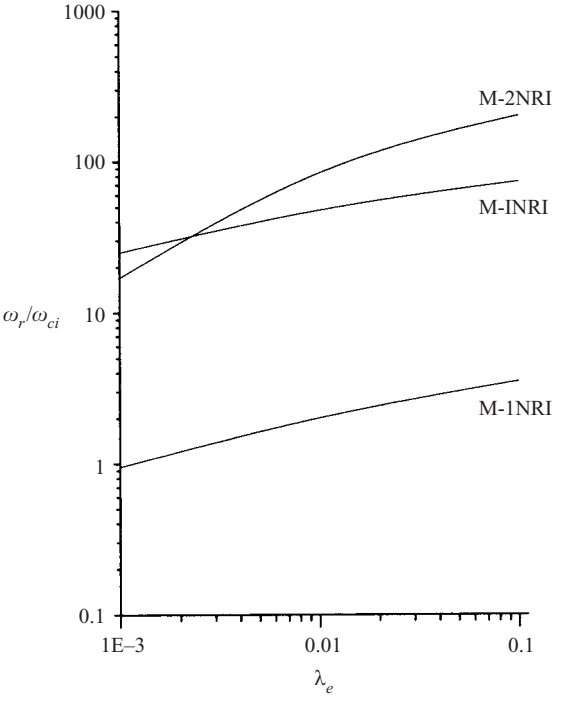


Figure 8. A plot of normalized ω_r vs λ_e for M-1, M-2 and M-I non-resonant instability.

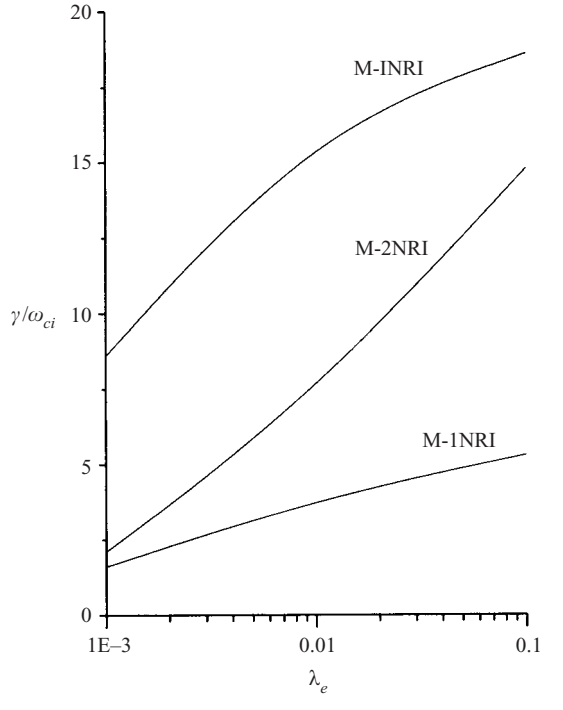


Figure 9. The growth rate curves for M-1, M-2 and M-I non-resonant instability corresponding to Fig. 8.

https://doi.org/10.1017/S002237780300223X Published online by Cambridge University Press

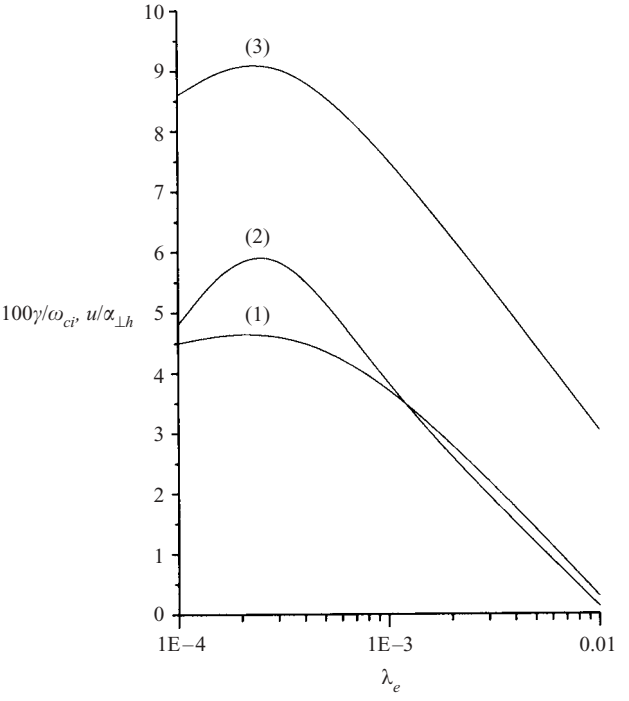


Figure 10. A plot of the normalized γ and ring speeds vs λ_e for the resonant instability. The growth rate curve (1) [(2)] corresponds to $\frac{u}{\alpha_{\perp h}} = 1.6$ [1.2], respectively. The curve (3) represents the critical value of drift speed required to excite the resonant instability.

5.3. The resonant instability

The resonant instability is excited for ring current parameters that are significantly different from those required for the excitation of M-1NRI but somewhat similar to those required for the excitation of M-2NRI.

Whereas in the non-resonant instability (both mode 1 and mode 2), T_e and T_h were set to be equal (200 eV) for the excitation of these modes, for the resonant instability, as discussed above, $T_h \gg T_e$ must be satisfied for excitation. In addition, a magnetic field value intermediate to mode 1 and mode 2 non-resonant instability is required for excitation. Wave propagation angles for the generation of this mode are in the range required by M-2NRI ($\theta \approx 80°$), compared with $\theta \approx 90°$ for the case of M-1NRI. In our computation, the hot and cold ion densities are set to exactly the same values as those used for the M-2NRI.

Standard parameters for the study of the resonant instability were as follows: $\theta = 82°$; $T_e = 0.375$ eV; $T_h = 7000$ eV; $B_0 = 134$ nT ($\omega_{ci} = 12.84\,\mathrm{rad\,s^{-1}}$); $N_{0c} = 65\,\mathrm{cm^{-3}}$; $N_{0h} = 1.6\,\mathrm{cm^{-3}}$; $u/\alpha_{\perp h} = 1.2$ (only used in the evaluation of γ since ω_r is independent of this ratio).

In Fig. 10, for the relevant above fixed parameters, the curve (3) represents the critical value of drift speed $u/\alpha_{\perp h}$, required to excite the resonant instability. Values of u in the range 0.3–1.0$\alpha_{\perp h}$ correspond to actual ring speeds of $u = 400$–$1160\,\mathrm{km\,s^{-1}}$. The curves (1) and (2) are growth rate curves obtained for the standard parameters mentioned above, except that the value of $u/\alpha_{\perp h}$ corresponds to $u/\alpha_{\perp h} = 1.6$ and 1.2, respectively. The real frequency is found to be unaffected

https://doi.org/10.1017/S002237780300223X Published online by Cambridge University Press

by a change in the parameter $u/\alpha_{\perp h}$, in agreement with the approximate analytical solution for ω_r as given in (19). The curves are consistent with those obtained by Singh et al. (1996). For $u/\alpha_{\perp h} = 1.2$ and 1.6 (curves 2 and 1), Fig. 10 predicts maximum growth rates of $f_{\gamma_{max}} = \gamma_{max}/2\pi = 0.14$ and 0.096 Hz, respectively. It is noted that the resonant instability is dominant in a lower range of λ_e values in comparison to the non-resonant instability.

The variation of the real frequency and growth rate of the resonant instability with the (cool) electron temperature are found to be similar to Figs 1 and 2 for the M-1NRI, except that ω_r and γ were two orders of magnitude larger in the case of the resonant instability. A similar behaviour is seen for the variation of the magnetic field strength.

6. Conclusion

Using linear kinetic theory, we have derived and solved the dispersion relation for low-frequency, electromagnetic instabilities excited in the ring current region of the Earth's magnetosphere. Our model is based on that of Singh et al. (1996). The mode 1 and mode 2 non-resonant instabilities were investigated as well as an intermediate non-resonant mode. In addition, a resonant instability was studied. Each of the instabilities (both resonant and non-resonant) discussed were found to exhibit significant growth over a certain range of λ_e values. The resonant instability showed most significant growth in the range $\lambda_e = 0.0001$–0.01, while each of the two non-resonant instabilities (mode 1 and mode 2) were excited in the range $\lambda_e = 0.001$–0.1.

It must be stressed that each mode discussed will only be excited for a certain range of parameters. For M-1NRI and M-2NRI, $T_e/T_h \approx 1$, while for the resonant instability, $T_e/T_h \ll 1$, were the requirements for the electron and hot ion temperatures. The condition for the hot and cold ion densities were the same for M-2NRI and the resonant instability ($N_{0c}/N_{0h} \gg 1$), while the opposite condition applied for M-1NRI ($N_{0c}/N_{0h} \ll 1$). M-1NRI was excited for smaller values of magnetic fields ($B_0 \approx 80$ nT), compared with M-2NRI ($B_0 \approx 320$ nT). The resonant instability required magnetic field strengths in between these values.

In general, the mode 2 non-resonant instability dominates the mode 1 non-resonant instability in terms of the real frequency. However, the reverse applies to the growth rate. The real frequency value ranges obtained for the resonant mode, are very much similar to those for the mode 2 non-resonant instability. The growth rates, however, are very much smaller.

Both M-1NRI and M-2NRI show the same trend in behaviour as a function of the electron temperature. In both cases, lower electron temperatures show a larger real frequency and growth rate for any λ_e in the studied range. Hence, the choice of electron temperatures by Singh et al. (1996) (200 eV for M-1NRI and M-2NRI, 0.375 eV for the resonant instability) are indeed justified. Furthermore, only for low electron temperatures (0.3–3 eV), does the growth rate of the resonant instability peak within the λ_e range studied.

M-1NRI, M-2NRI and the resonant instability show the same trends with regard to magnetic field strength variations. In each case, there is an increase in real frequency and growth rate with an increase in $|\mathbf{B}_0|$. This is due to the larger magnetic fields having more influence on the magnetized particles, thereby restricting their motion across $\mathbf{B}_0$ and enhancing the instability.

https://doi.org/10.1017/S002237780300223X Published online by Cambridge University Press

The solution to the complete dispersion relation for intermediate parameters (with respect to those chosen separately for the M-1NRI and the M-2NRI) give larger growth rates than those for the M-1NRI and the M-2NRI for the typical λ_e range chosen for the non-resonant instability studies. The real frequencies, however, lie between each of the two modes (for $\lambda_e > 0.005$) and are significantly closer to M-2NRI.

References

Abramowitz, M. and Stegun, I. A. 1964 *Handbook of Mathematical Functions*, *Appl. Math. Series*, Vol. 55, National Bureau of Standards. Washington, DC: US Government Printing Office.

Bhatia, K. G. and Lakhina, G. S. 1980 *Proc. Indian Acad. Sci. (Earth Planet. Sci.)* **89**, 99.

Fritz, T. A. and Spjeldvik, W. N. 1979 *J. Geophys. Res.* **84**, 2608.

Kistler, L. M., Mobius, E., Klecker, B., Gloeckler, G., Ipavich, F. M. and Hamilton, D. C. 1990 *J. Geophys. Res.* **95**, 18 871.

Laakso, H., Junginger, H., Roux, A., Schmidt, R. and de Villedary, C. 1990 *J. Geophys. Res.* **95**, 10 609.

Lui, A. T. Y., McEntire, R. W., Sibeck, D. G. and Krimigis, S. M. 1990 *J. Geophys. Res.* **95**, 20 839.

McClements, K. G. and Dendy, R. O. 1994 *J. Geophys. Res.* **98**, 11 689.

Parks, G. K. 1991 *Physics of Space Plasmas – an Introduction*. Reading, MA: Addison-Wesley.

Perraut, S., Roux, A., Robert, P., Gendrin, R., Sauvard, J. A., Bosqued, J. M., Kremser, G. and Korth, A. 1982 *J. Geophys. Res.* **87**, 6219.

Singh, S. V., Bharuthram, R. and Lakhina, G. S. 1996 *Earth, Moon Planets* **74**, 231.

https://doi.org/10.1017/S002237780300223X Published online by Cambridge University Press